Rare Met. (2020) 39(2):131–138
https://doi.org/10.1007/s12598-019-01341-z

RARE METALS
www.editorialmanager.com/rmet

Improved open-circuit voltage and ambient stability of $CsPbI_2Br$ perovskite solar cells by incorporating CH_3NH_3Cl

Chuan-Liang Chen, Sha-Sha Zhang, Tian-Lun Liu, Shao-Hang Wu, Zhi-Chun Yang, Wei-Tao Chen, Rui Chen, Wei Chen*

Received: 20 February 2019 / Revised: 25 March 2019 / Accepted: 23 September 2019 / Published online: 9 December 2019

Abstract Inorganic cesium metal halide perovskites have gained research interest as absorbers in perovskite solar cells due to their superior thermal stability. Among these, $CsPbI_2Br$, with a narrower band gap than $CsPbBr_3$ and a better phase stability than $CsPbI_3$, has received tremendous interest of the researchers. However, $CsPbI_2Br$ takes adverse phase transfer easily with an exposure to the water vapor in ambient air which not only brings inconvenience for researches but also puts forward very high requirement for encapsulation. Herein, a dense and uniform film is obtained by incorporating hydrophobic CH_3NH_3Cl (MACl) into the precursor solution. Being attributed to a good passivation effect, the defect density is decreased from 3.12×10^{16} to 1.49×10^{16} cm^{-3} and the average photoluminescence lifetime is increased from 8.84 to 20.6 ns. The photovoltaic device achieves a high open-circuit voltage of 1.22 V based on optimized MACl-doped film and accordingly a higher power conversion efficiency (PCE) of 12.9% which is 21.7% higher than the pristine $CsPbI_2Br$ device with PCE of 10.6%. In addition, the ambient stability of MACl-doped device has been enhanced, which is greatly attributed to the hydrophobic properties of MACl. This work provides a clue to improve ambient stability of inorganic perovskite solar cells and inspires toward further development of this material.

Keywords $CsPbI_2Br$ perovskite; Passivation; Ambient stability; MACl

Chuan-Liang Chen and Sha-Sha Zhang have contributed equally to this work.

Electronic supplementary material The online version of this article (https://doi.org/10.1007/s12598-019-01341-z) contains supplementary material, which is available to authorized users.

C.-L. Chen, S.-S. Zhang, S.-H. Wu, Z.-C. Yang, W.-T. Chen, R. Chen, W. Chen*
Wuhan National Laboratory for Optoelectronics, Huazhong University of Science and Technology, Wuhan 430074, China
e-mail: wnlochenwei@mail.hust.edu.cn

T.-L. Liu
China-EU Institute for Clean and Renewable Energy, Huazhong University of Science and Technology, Wuhan 430074, China

W. Chen
Shenzhen Key Laboratory of Nanobiomechanics, Shenzhen Institutes of Advanced Technology, Chinese Academy of Sciences, Shenzhen 518055, China

1 Introduction

Hybrid organic–inorganic halide perovskite solar cells have been considered as a promising photovoltaic technology with a rapid rise in power conversion efficiency (PCE) from 3.8% to 22.7% and a low cost for fabrication by solution process [1–5]. A major obstacle to commercialization is their instability. In particular, they subject to compositional degradation at high temperature [6]. It has been reported that when $MAPbI_3$ is annealed above 85 °C, it can be significantly decomposed into PbI_2 and MAI [7]. One promising way to enhance their thermal stability is to substitute the organic component ($CH_3NH_3^+$, $NH_2CH=NH_2^+$) with an inorganic component such as Cs [8–10]. Accordingly, $CsPbI_3$, due a suitable band gap of 1.73 eV, has been developed for photovoltaic application and the based solar cells have been fabricated with a PCE of 2.9% by Snaith and coworkers [11]. Unfortunately, $CsPbI_3$ is unstable in the black cubic phase at room temperature which will quickly convert to the yellow nonperovskite phase, especially in ambient atmosphere. Meanwhile, $CsPbBr_3$ has also been used as absorber in solar cells and a PCE of 6% has been achieved by Kulbak et al. [12, 13]. However, the band gap of $CsPbBr_3$ is 2.3 eV, which is too wide to be used even in multi-junction tandem solar cells [14]. Hence, a series of $CsPbI_{3-x}Br_x$ perovskite has been developed in order to obtain both suitable band gap and high phase stability simultaneously [15–21]. Among these, $CsPbI_2Br$, with a band gap of $\sim$1.9 eV, is suitable for a top block in a triple-junction device and accordingly has been concerned by many researchers [22–28]. Up to now, $CsPbI_2Br$-based regular solar cells have achieved PCE as high as 13.47% and show excellent stability at both room and elevated temperatures when prevented from exposure to water vapor [29]. However, there is still large energy loss, reflected by the large difference between band gap (E_g) and open-circuit voltage (V_{OC}), especially for devices with inverted structures. Furthermore, the bad humidity stability puts forward high requirement for encapsulation, brings large inconvenience and increased cost for study and hinders its further development and potential application in the future.

In this paper, we incorporated a small amount of hydrophobic material of CH_3NH_3Cl (MACl) to $CsPbI_2Br$ precursor solution. The influences of the MACl content on the morphology and defect density of the perovskite film as well as the final device performance were studied carefully. Ultraviolet–visible (UV–Vis) spectra and X-ray photoelectron spectroscopy (XPS) characterization were also conducted to analyze the band gap and composition changes. Furthermore, the stability of $CsPbI_2Br$ solar cells based on MACl additive was tested, which is much better than that of the pristine device. This work provides useful information about perovskite solar cells and is an advance of practical applications to cater the current energy need of the world.

2 Experimental

2.1 Device fabrication

Glass substrates (TEC-15, NSG Pilkington) with the etched fluorine-doped tin oxide (FTO) coating were first ultrasonically cleaned with detergent solution, Milli-Q water, ethyl alcohol and acetone in sequence. After drying with clean dry air, a p-type NiMgLiO film serving as hole extraction layer was deposited onto FTO glass by spray pyrolysis at 550 °C according to our previous work [30]. Then, the NiMgLiO-coated FTO glass substrates were transferred to a N_2-filled glove box. The anti-solvent-assisted spin-coating technology was used for the deposition of $CsPbI_2Br(MACl)_x$-based perovskite layers: 0.85 $mol{\cdot}L^{-1}$ dimethylformamide (DMF)/dimethyl sulfoxide (DMSO) (4:1 by volume ratio) mixture solution of PbI_2/CsBr/MACl (1:1: x by molar ratio, x = 0, 0.01, 0.03, 0.05, 0.08) was spin-coated at 4000 $r{\cdot}min^{-1}$ for 45 s, followed by rapidly drop-casting diethyl ether (1 ml) as anti-solution, and then annealed at 240 °C for 20 s. The formed perovskites were denoted as MACl 0, MACl 0.01, MACl 0.03, MACl 0.05, and MACl 0.08, respectively. After the inorganic perovskite films were prepared, a chlorobenzol solution of [6]-phenyl-C61-butyric acid methyl ester (PCBM) (20 $mg{\cdot}ml^{-1}$) was spin-coated on top of them at the rotation speed of 2000 $r{\cdot}min^{-1}$ for 30 s. Subsequently, a 5-nm-thick buffer layer was fabricated by spin-coating saturated methanol solution of BCP at the rotation speed of 6000 $r{\cdot}min^{-1}$ for 30 s. Finally, 120-nm-thick Ag electrodes were deposited under high vacuum ($< 5 \times 10^{-4}$ Pa) in evaporation chamber.

2.2 Characterization

Scanning electron microscopy (SEM) images were obtained via a Nova Nano 450 SEM (FEI Co., the Netherlands) at a 5 kV accelerating voltage. X-ray diffraction (XRD) characterization was performed on a Philips X-ray diffractometer with Cu Kα radiation. X-ray photoelectron spectroscopy (XPS) measurements were carried out on an AXIS-ULTRA DLD-600W Ultra spectrometer (Kratos Co., Japan). The ultraviolet–visible (UV–Vis) spectra were obtained from a Lambda 950 spectrophotometer (PerkinElmer Co., USA). The PL spectra were performed on an Edinburgh FLS920 fluorescence spectrometer (Edinburgh Co., UK). The current density–voltage (J–V) curves were measured via a Keithley 2400 source meter. A solar simulator (Oriel, model 9119) with AM 1.5G filter (Oriel, model 91192) was used to provide an irradiance of 100 $mW{\cdot}cm^{-2}$, and the light intensity of the simulated solar light was precisely calibrated with a standard Si photodiode detector. The effective area of the solar cell was defined to be 0.09 cm^2 with a black metal mask. The incident photo-to-electron conversion efficiency (IPCE) was measured on a Newport IPCE system (Newport, USA). The Mott–Schottky plots were obtained via an electrochemical workstation (Zahner Zennium, Germany).

3 Results and discussion

Based on anti-solvent method, $CsPbI_2Br$ films with varying MACl contents were fabricated. To investigate the effect of different MACl additions on the surface morphology of perovskite films, top-view SEM images were processed and the results are shown in Fig. 1. It is found that the changes are not manifest among the perovskite films when

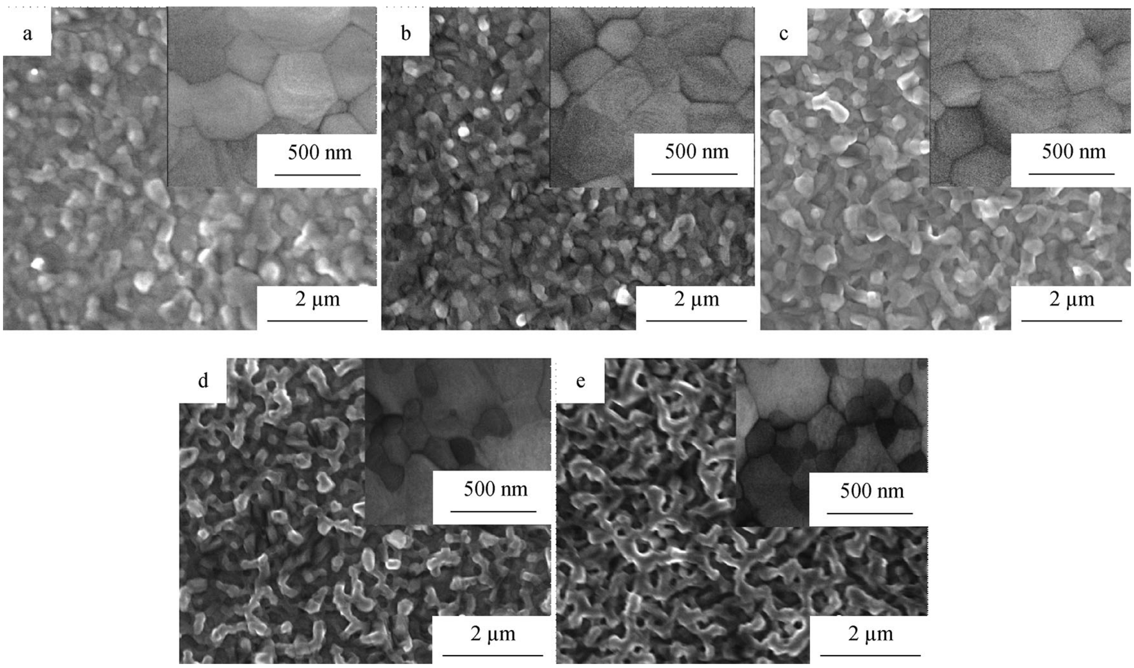

Fig. 1 Surface SEM images of $CsPbI_2Br(MACl)_x$ films: **a** $x = 0$, **b** $x = 0.01$, **c** $x = 0.03$, **d** $x = 0.05$ and **e** $x = 0.08$

the MACl content varies from 0 to 0.03, while if the MACl content is further increased to more than 0.05, the $CsPbI_2Br$ film becomes inhomogeneous and lots of small grains emerge (Fig. 1d, e). Such results indicate that moderate MACl additive is beneficial for the interface passivation and assists in achieving high-quality inorganic perovskite films.

XRD measurements are provided to quantify the effect of MACl additive on the crystallinity of $CsPbI_2Br$ film, and the results are depicted in Fig. 2. It is noted that all the MACl-doped films show a typical perovskite phase with the dominant peaks at 14.6° and 29.5°, assigned to (100) and (200) planes, respectively, which is well consistent with previous studies [28, 31]. Upon MACl doping, all the inorganic perovskites demonstrate similar XRD patterns, indicating that small amount of MACl doping does not change the growth direction of $CsPbI_2Br$ crystals. In addition, it is found that the absolute intensities of both the two peaks for all those patterns decrease apparently with the increase in MACl content. These results coherently indicate that MACl additive has a significant influence on the grain growth and litter size grains emerge with the MACl additive increasing, which are confirmed by the SEM images in Fig. 1.

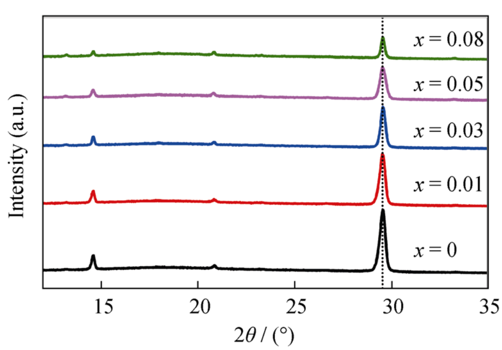

Fig. 2 XRD patterns of $CsPbI_2Br(MACl)_x$ films with varying MACl contents

For the purpose of understanding the effect of MACl additive on the elemental composition at the surface of inorganic perovskite films, XPS measurements were carried out on the $CsPbI_2Br$ and $CsPbI_2Br(MACl)_{0.03}$ films. The results are shown in Fig. S1. Obvious peak of Cl element centered at 198.2 eV is observed for the $CsPbI_2Br(MACl)_{0.03}$ film. Furthermore, there is a little shift for Pd 4f peaks toward lower binding energy, indicating that Pb–Cl bonds may be formed in the lattice. Atomic ratios are listed in Table S1. As seen, the Cl/Pb atomic ratio is about 3.2%, close to the molar content of MACl additive. Meanwhile, the reduced I/Pb atomic ratios are estimated to be 221% for the $CsPbI_2Br(MACl)_{0.03}$ film, far less than 247% for the $CsPbI_2Br$ film, which means that partial I^- has been substituted by Cl^-. Based on XPS results within the typical XPS detection depth of 10 nm, it is noted that the content of C increases sharply after incorporating 0.03 mol% MACl into $CsPbI_2Br$ film, which means that a great deal of MA^+ stays at the surface of inorganic film as a passivator. The results indicate that MA^+ is enriched at MACl-doped film surfaces, which can passivate defect states at the surface, quite similar to our previous study on Ca^{2+}-doped perovskite films [32].

Optical and PL measurements were also conducted on the $CsPbI_2Br(MACl)_x$ films, and the results are presented in Fig. 3. Figure 3a demonstrates that with the increase in MACl content from 0 to 0.03, the corresponding UV–Vis spectroscopy shows an apparent blueshift and their absorption onsets shift gradually from 656 nm ($\sim$ 1.9 eV) to 636 nm ($\sim$ 1.95 eV). In contrast, if the MACl content further increases to 0.08, the corresponding absorption peak positions keep almost constant, suggesting that it has been saturated for MACl doping just with a little content of 0.03. At the same time, with the MACl content further increasing, the absorption of the inorganic film slightly degrades which may be attributed to large number of small grains demonstrated by SEM.

Steady-state photoluminescence (PL) spectra for $CsPbI_2Br(MACl)_x$ films on glass substrates are given in Fig. 3b. They exhibit apparent blueshift with MACl content increasing from 0 to 0.08, attributed to insertion of Cl^- to the lattice of $CsPbI_2Br$ perovskite, which is in good agreement with the UV–Vis results. At the same time, their peak intensity increases first and then decreases with the increase in MACl content and achieves the maximum intensity for the 0.03 MACl additive. These results suggest that 0.03 MACl-doped film has the least defect states, which is consistent with their improved morphology and abrupt slope of UV–Vis absorption.

The improvement in the steady PL intensity usually relates to prolonged carrier lifetime, which can be verified by time-resolved PL spectra depicted in Fig. 3c. Herein, the time-resolved PL decay curve can be fitted with following bi-exponential decay function [33]:

$$F(t) = A_1 \exp\left(-\frac{t}{\tau_1}\right) + A_2 \exp\left(-\frac{t}{\tau_2}\right) \quad (1)$$

where F is the normalized intensity; t is the time; τ_1, τ_2 are lifetimes related to two kinds of recombination; and A_1 and A_2 are the related weight contents. The average decay time (mean PL average lifetime) can be obtained by the following equation:

$$\tau_{avg} = \frac{A_1\tau_1 + A_2\tau_2}{A_1 + A_2} \quad (2)$$

where τ_{avg} denotes the average decay time. With variation in the content of MACl additive, the fitting parameters (τ_1, τ_2, A_1, A_2) and PL average lifetime are summarized in Table S2. Obviously, the PL lifetime for MACl 0.03 additive film is 20.6 ns, much larger than that for pristine $CsPbI_2Br$ film (8.84 ns) and MACl 0.08 additive film (1.11 ns). This result indicates that moderate MACl doping may be useful for improving optoelectronic properties of inorganic $CsPbI_2Br$ perovskite film.

Based on MACl-doped films, perovskite solar cells (PSCs) with inverted architecture of "FTO/NiMgLiO/$CsPbI_2Br(MACl)_x$/PCBM/BCP/Ag" (Fig. 4a) have been fabricated. Their J–V characteristic curves of the champion samples under AM 1.5 G irradiation at 100 mW·cm^{-2} are demonstrated in Fig. 4b, and the resultant performance parameters are listed in Table S3. At the same time, the statistic distribution of performance parameters depending on MACl additive content is presented in Fig. 4c–f. In this study, the champion cell based on 0.03 MACl additive exhibits the highest power conversion efficiency (PCE) of 12.9%, with an open-circuit voltage (V_{OC}) of 1.22 V, a short-circuit current density (J_{SC}) of 13.8 mA·cm^{-2} and a fill factor (FF) of 0.76. However, the $CsPbI_2Br$-based cell only obtains a PCE of 10.6%, with V_{OC} of 1.08 V, J_{SC} of 14.4 mA·cm^{-2} and FF of 0.68. Obviously, the main enhancement in PCE of 0.03 MACl device comes from enhanced V_{OC} and FF due to better morphology and wider band gap. It is noteworthy that if the MACl content further increases from 0.03 to 0.08, V_{OC}, J_{SC} and FF decrease significantly to 0.95 V, 12.6 mA·cm^{-2} and 0.62, respectively, resulting in a much degraded PCE of 7.4%. Such result may be attributed to poor morphology with excessive MACl additive. Furthermore, it is found that the device based on 0.03 MACl content exhibits little hysteresis compared to pristine $CsPbI_2Br$-based device (Fig. S2),

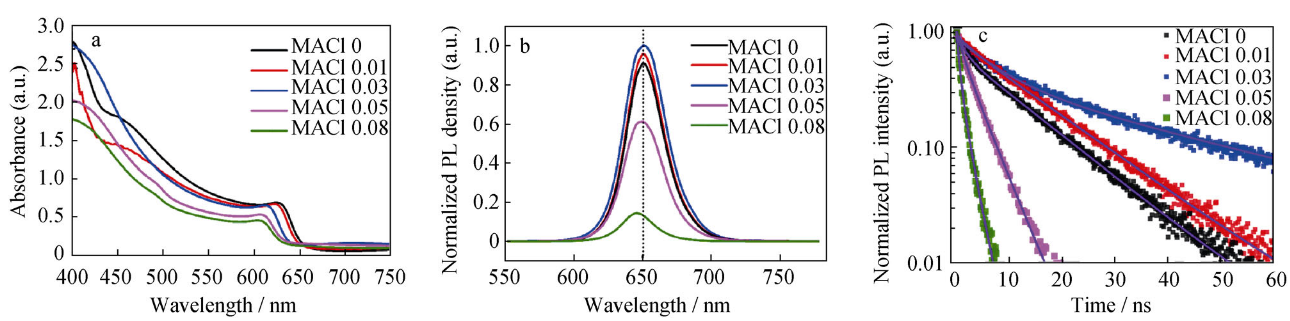

Fig. 3 **a** UV–Vis absorption spectra; **b** steady-state PL spectra; and **c** normalized time-resolved PL spectra of $CsPbI_2Br(MACl)_x$ films with varying MACl contents on glass substrates

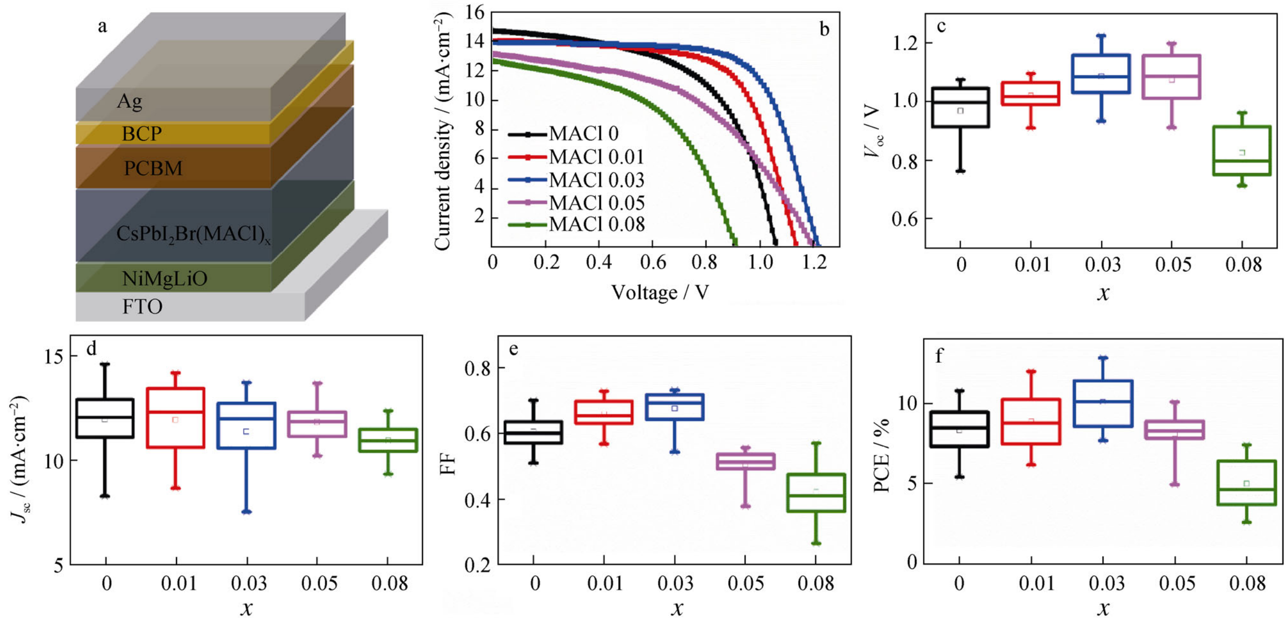

Fig. 4 **a** Device architecture of FTO/NiMgLiO/$CsPbI_2Br(MACl)_x$/PCBM/BCP/Ag; **b** *J–V* characteristics of champion devices based on $CsPbI_2Br(MACl)_x$ under forward scan direction; photovoltaic parameters of perovskite devices as a function of MACl additive content: **c** J_{SC}, **d** V_{OC}, **e** FF, **f** PCE (16 pieces of solar cells included)

which is attributed to the excellent carrier extraction capability of surface and trap passivation by MACl.

It is obviously found that the J_{SC} value for 0.03 MACl-doped device is 13.8 $mA \cdot cm^{-2}$, which is smaller than that for the pristine $CsPbI_2Br$-based device (14.4 $mA \cdot cm^{-2}$), matching well with the integrated J_{SC} values from the IPCE data presented in Fig. 5a. This result may be ascribed to the blueshift of absorption spectra, leading to a smaller cutoff wavelength.

Besides, V_{OC} of $CsPbI_2Br(MACl)_{0.03}$-based cell achieves a value of 1.22 V, much higher than that of pristine $CsPbI_2Br$-based cell (1.08 V) and $CsPbI_2Br(MACl)_{0.08}$-based cell (0.95 V). The higher *V*oc is partly attributed to the wider band gap of ~ 1.95 eV, but more importantly, the much-reduced defect density and more effective charge extraction at the surface may play a great role. To elucidate the origin of enhanced V_{OC}, Mott–Schottky analysis has been performed on the two photovoltaic devices based on $CsPbI_2Br$ and $CsPbI_2Br(MACl)_{0.03}$. Figure 5b presents the capacitance–voltage ($1/C^2 - V$) plots for the corresponding cells, and the built-in potentials (V_{bi}) can be acquired with the following Mott–Schottky equation [28]:

$$\frac{1}{C^2} = \frac{2}{\varepsilon\varepsilon_0 q A^2 N}(V_{bi} - V) \tag{3}$$

where V is the applied bias and the parameters ε, ε_0, q, A and N represent mean relative permittivity, vacuum permittivity, elementary charge, active area and free carrier concentration, respectively. Based on the method reported in our previous literature [27], the values of V_{bi} are equal to 0.64 and 0.94 V for the cells based on $CsPbI_2Br$ and $CsPbI_2Br(MACl)_{0.03}$, respectively (Fig. 5b). This result is

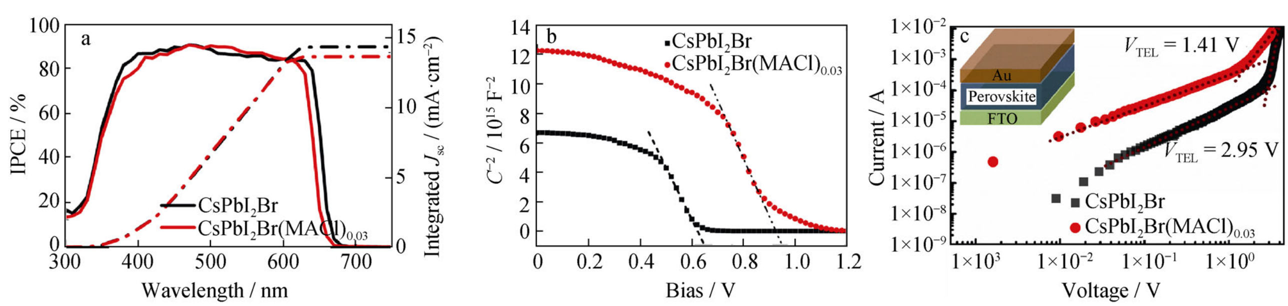

Fig. 5 **a** Incident photo-to-electron conversion efficiency (IPCE) curves (solid lines) with integrated photocurrents (dashed lines); **b** Mott–Schottky plots for champion devices based on $CsPbI_2Br$ and $CsPbI_2Br(MACl)_{0.03}$ films; **c** bilogarithmic diagram of *I–V* curves in dark for devices with architecture of FTO/perovskite/Au

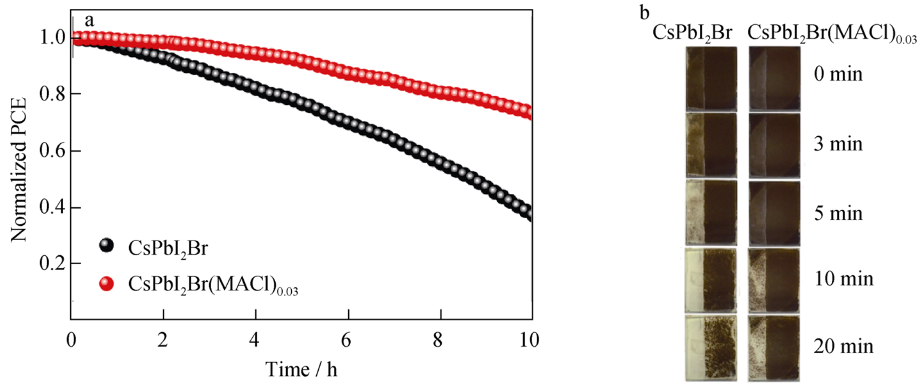

Fig. 6 **a** Normalized PCEs of unencapsulated photovoltaic devices based on $CsPbI_2Br$ and $CsPbI_2Br(MACl)_{0.03}$ films under continuous illumination (simulated solar light, 100 $mW{\cdot}cm^{-2}$), placed in ambient atmosphere with a humidity of ~ 30%; **b** comparison of degradation speeds from two different samples: $CsPbI_2Br$ film and $CsPbI_2Br(MACl)_{0.03}$ film, two films were all placed in ambient atmosphere for 20 min

consistent with the trend of V_{OC} values extracted from their *J*–*V* curves. A higher V_{bi} means an improved driving force for the separation of photo-generated carriers and an extended depletion region for efficient suppression of electron–hole recombination. As a result, the incorporation of small amount of MACl is beneficial to the increase in the output voltage of $CsPbI_2Br$ PSCs.

To further elucidate the impact of MACl addition on perovskite trap density, the *I*–*V* responses of two samples based on $CsPbI_2Br$ and $CsPbI_2Br(MACl)_{0.03}$, with the architecture of FTO/perovskite/Au, have been performed [34, 35]. Their dark current–voltage (*I*–*V*) characteristic curves are presented in Fig. 5c. Herein, the trap-filled limit voltage (V_{TFL}) can be used to calculate the trap state density (N_{trap}) with the equation of $N_{trap} = V_{TFL}\ (2\varepsilon\varepsilon_0)/eL^2$, where e is the elementary charge (1.6×10^{-19} C), L is the perovskite film thickness (~ 300 nm), the vacuum permittivity (ε_0) is equal to 8.854×10^{-12} $F{\cdot}m^{-1}$ and the relative permittivity (ε) for $CsPbI_2Br$ perovskite is ~ 8.6 [36]. From Fig. 5c, it can be determined that V_{TFL} for samples based on $CsPbI_2Br$ and $CsPbI_2Br(MACl)_{0.03}$ is 2.95 and 1.41 V, respectively. The resultant N_{trap} is calculated to be 3.12×10^{16} and 1.49×10^{16} cm^{-3}, respectively. Obviously, the trap state densities are decreased after the $CsPbI_2Br$ film is passivated by MACl. It is noted that the enhanced quality of perovskite films is consistent with the corresponding steady PL and time-resolved PL spectra depicted in Fig. 3b, c.

In addition to device efficiency, the ambient stability of devices based on $CsPbI_2Br$ and $CsPbI_2Br(MACl)_{0.03}$ films is also examined. Figure 6a shows the normalized PCEs of unencapsulated devices under continuous illumination (simulated solar light, 100 $mW{\cdot}cm^{-2}$) in ambient atmosphere ($T = \sim 25$ °C and relative humidity (RH) = ~ 30%). It is found that the $CsPbI_2Br(MACl)_{0.03}$ device retains 80% of its initial efficiency for ~ 8.1 h, nearly 1.8 times that for $CsPbI_2Br$ device (~ 4.4 h). The enhanced ambient stability may be partially attributed to interface passivation; moreover, the incorporated MACl additive as a hydrophobic material may play an important role. Herein, two different devices, namely FTO/NiMgLiO/$CsPbI_2Br$ and FTO/NiMgLiO/$CsPbI_2Br(MACl)_{0.03}$, were fabricated and compared under their optimal interfacial condition. As demonstrated in Fig. 6b, when the two devices were placed in ambient atmosphere, the pristine $CsPbI_2Br$ perovskite layer was corroded rapidly within ~ 3 min, while the $CsPbI_2Br(MACl)_{0.03}$ layer was kept nearly undamaged for ~ 10 min. Thus, the much stable $CsPbI_2Br(MACl)_{0.03}$ layer gives the device higher stability in ambient atmosphere.

4 Conclusion

In summary, the effects of MACl on $CsPbI_2Br$ perovskite films and the based devices were investigated. With the incorporation of a small amount of MACl (≤ 0.03), $CsPbI_2Br$ perovskite films demonstrate denser and uniform morphology and achieve the best state when the MACl content is equal to 0.03. Being attributed to a good passivation effect, the defect density decreases dramatically and the average PL lifetime increases to 20.6 ns. Based on such optimized MACl-doped films, the champion cell achieves a PCE of 12.9% with much higher V_{oc} of 1.22 V compared to the pristine $CsPbI_2Br$ cells, with the V_{oc} of 1.08 V. In addition, compared with the $CsPbI_2Br$-based device, the $CsPbI_2Br(MACl)_{0.03}$-based cell reveals a superior ambient stability, which is attributed to the improved perovskite quality and better hydrophobic characteristics of $CsPbI_2Br(MACl)_{0.03}$ layers. This work provides a clue for improving ambient stability of inorganic perovskite cells, which is of particular importance for practical application.

Acknowledgements This work was financially supported by the National Natural Science Foundation of China (Nos. 51672094, 51861145404 and 51822203), the China Postdoctoral Science Foundation (No. 2016M602286), the Self-determined and Innovative Research Funds of HUST (No. 2016JCTD111), Shenzhen Science and Technology Innovation Committee (No. JCYJ2017030716590 5513) and the Natural Science Foundation of Guangdong Province (No. 2017A030313342). The authors appreciate Analytical and Testing Center of Huazhong University of Science and Technology for the sample measurements.

References

[1] Kojima A, Teshima K, Shirai Y, Miyasaka T. Organometal halide perovskites as visible-light sensitizers for photovoltaic cells. J Am Chem Soc. 2009;131(17):6050.

[2] Mao G, Wang W, Shao S, Sun X, Chen S, Li M, Li H. Research progress in electron transport layer in perovskite solar cells. Rare Met. 2018;37(2):95.

[3] Jeon NJ, Noh JH, Kim YC, Yang WS, Ryu S, Seok SI. Solvent engineering for high-performance inorganic-organic hybrid perovskite solar cells. Nat Mater. 2014;13(9):897.

[4] Yang WS, Noh JH, Jeon NJ, Kim YC, Ryu S, Seo J, Seok SI. SOLAR CELLS. High-performance photovoltaic perovskite layers fabricated through intramolecular exchange. Science. 2015;348(6240):1234.

[5] Yang WS, Park BW, Jung EH, Jeon NJ, Kim YC, Lee DU, Shin SS, Seo J, Kim EK, Noh JH, Seok SI. Iodide management in formamidinium-lead-halide-based perovskite layers for efficient solar cells. Science. 2017;356(6345):1376.

[6] Conings B, Drijkoningen J, Gauquelin N, Babayigit A, D'Haen J, D'Olieslaeger L, Ethirajan A, Verbeeck J, Manca J, Mosconi E, Angelis FD, Boyen HG. Intrinsic thermal instability of methylammonium lead trihalide perovskite. Adv Energy Mater. 2015;5(15):1500477.

[7] Kim J, Park N, Yun JS, Huang S, Green MA, Ho-Baillie AWY. An effective method of predicting perovskite solar cell lifetime–Case study on planar $CH_3NH_2PbI_3$ and $HC(NH_2)_2PbI_3$ perovskite solar cells and hole transfer materials of spiro-OMeTAD and PTAA. Sol Energy Mater Sol Cells. 2017;162:41.

[8] Sutton RJ, Eperon GE, Miranda L, Parrott ES, Kamino BA, Patel JB, Hörantner MT, Johnston MB, Haghighirad AA, Moore DT, Snaith HJ. Bandgap-tunable cesium lead halide perovskites with high thermal stability for efficient solar cells. Adv Energy Mater. 2016;6(8):1502458.

[9] Frolova LA, Anokhin DV, Piryazev AA, Luchkin SY, Dremova NN, Stevenson KJ, Troshin PA. Highly efficient all-inorganic planar heterojunction perovskite solar cells produced by thermal coevaporation of CsI and PbI_2. J Phys Chem Lett. 2017;8(1):67.

[10] Choi H, Jeong J, Kim HB, Kim S, Walker B, Kim GH, Kim JY. Cesium-doped methylammonium lead iodide perovskite light absorber for hybrid solar cells. Nano Energy. 2014;7:80.

[11] Eperon GE, Paterno GM, Sutton RJ, Zampetti A, Haghighirad AA, Cacialli F, Snaith HJ. Inorganic caesium lead iodide perovskite solar cells. J Mater Chem A. 2015;3(39):19688.

[12] Kulbak M, Cahen D, Hodes G. How important is the organic part of lead halide perovskite photovoltaic cells? Efficient CsPbBr 3 cells. J Phys Chem Lett. 2015;6(13):2452.

[13] Kulbak M, Gupta S, Kedem N, Levine I, Bendikov T, Hodes G, Cahen D. Cesium enhances long-term stability of lead bromide perovskite-based solar cells. J Phys Chem Lett. 2016;7(1):167.

[14] Bremner SP, Yi C, Almansouri I, Ho BA, Green MA. Optimum band gap combinations to make best use of new photovoltaic materials. Sol Energy. 2016;135:750.

[15] Bian H, Bai D, Jin Z, Wang K, Liang L, Wang H, Zhang J, Wang Q, Liu S. Graded bandgap $CsPbI_{2+x}Br_{1-x}$ perovskite solar cells with a stabilized efficiency of 14.4%. Joule. 2018;2(8):1500.

[16] Lau CFJ, Deng X, Ma Q, Zheng J, Yun JS, Green MA, Huang S, Ho-Baillie AWY. $CsPbIBr_2$ perovskite solar cell by spray-assisted deposition. ACS Energy Lett. 2016;1(3):573.

[17] Bai DL, Bian H, Jin ZW, Wang HR, Meng LN, Wang Q, Liu SZ. Temperature-assisted crystallization for inorganic $CsPbI_2Br$ perovskite solar cells to attain high stabilized efficiency 14.81%. Nano Energy. 2018;52:408.

[18] Wang K, Jin Z, Liang L, Bian H, Bai D, Wang H, Zhang J, Wang Q, Liu S. All-inorganic cesium lead iodide perovskite solar cells with stabilized efficiency beyond 15%. Nat Commun. 2018;9:4544.

[19] Gao Y, Dong Y, Huang K, Zhang C, Liu B, Wang S, Shi J, Xie H, Huang H, Xiao S, He J, Gao Y, Hatton Ross A, Yang J. Highly efficient, solution-processed $CsPbI_2Br$ planar heterojunction perovskite solar cells via flash annealing. ACS Photonics. 2018;10:4104.

[20] Jae KN, Myung SJ, Sung UC, Yung JC, Dongho K, Jong HP. Unveiling the crystal formation of cesium lead mixed-halide perovskites for efficient and stable solar cells. J Phys Chem Lett. 2017;8(13):2936.

[21] Zhang SS, Wu SH, Chen WT, Zhu HM, Xiong ZZ, Yang ZC, Chen CL, Chen R, Han LY, Chen W. solvent engineering for efficient inverted perovskite solar cells based on inorganic $CsPbI_2Br$ light absorber. Mater Today Energy. 2018;8:125.

[22] Beal RE, Slotcavage DJ, Leijtens T, Bowring AR, Belisle RA, Nguyen WH, Burkhard GF, Hoke ET, McGehee MD. Cesium lead halide perovskites with improved stability for tandem solar cells. J Phys Chem Lett. 2016;7(5):746.

[23] Zeng Q, Zhang X, Feng X, Lu S, Chen Z, Yong X, Redfern SAT, Wei H, Wang H, Shen H, Zhang W, Zheng W, Zhang H, Tse JS, Yang B. Polymer-passivated inorganic cesium lead mixed-halide perovskites for stable and efficient solar cells with high open-circuit voltage over 1.3 V. Adv Mater. 2018;30(9):1705393.

[24] Niezgoda JS, Foley BJ, Chen AZ, Choi JJ. Improved charge collection in highly efficient $CsPbBrI_2$ solar cells with light-induced dealloying. ACS Energy Lett. 2017;2(5):1043.

[25] Chen CY, Lin HY, Chiang KM, Tsai WL, Huang YC, Tsao CS, Lin HW. All-vacuum-deposited stoichiometrically balanced inorganic cesium lead halide perovskite solar cells with stabilized efficiency exceeding 11. Adv Mater. 2017;29(12):1605290.

[26] Ma Q, Huang S, Wen X, Green MA, Ho BAWY. Hole transport layer free inorganic $CsPbIBr_2$ perovskite solar cell by dual source thermal evaporation. Adv Energy Mater. 2016;6(7):1502202.

[27] Liu C, Li W, Zhang C, Ma Y, Fan J, Mai Y. All-inorganic $CsPbI_2Br$ perovskite solar cells with high efficiency exceeding 13. J Am Chem Soc. 2018;140(11):3825.

[28] Lau CFJ, Zhang M, Deng X, Zheng J, Bing J, Ma Q, Kim J, Hu L, Green MA, Huang S, Ho BA. Strontium-doped low-temperature-processed $CsPbI_2Br$ perovskite solar cells. ACS Energy Lett. 2017;2(10):2319.

[29] Bai D, Zhang J, Jin Z, Bian H, Wang K, Wang H, Liang L, Wang Q, Liu SF. Interstitial Mn^{2+}-driven high-aspect-ratio grain growth for low-trap-density microcrystalline films for record efficiency $CsPbI_2Br$ solar cells. ACS Energy Letters. 2018;3(4):970.

[30] Chen W, Wu Y, Yue Y, Liu J, Zhang W, Yang X, Chen H, Bi E, Ashraful I, Gratzel M, Han L. Efficient and stable large-area perovskite solar cells with inorganic charge extraction layers. Science. 2015;350(6263):944.

[31] Lau CFJ, Deng X, Zheng J, Kim J, Zhang Z, Zhang M, Bing J, Wilkinson B, Hu L, Patterson R, Huang S, Ho BA. Enhanced performance via partial lead replacement with calcium for a $CsPbI_3$ perovskite solar cell exceeding 13% power conversion efficiency. J Mater Chem A. 2018;6(14):5580.

[32] Chen C, Xu Y, Wu S, Zhang S, Yang Z, Zhang W, Zhu H, Xiong Z, Chen W, Chen W. CaI_2: a more effective passivator of perovskite films than PbI_2 for high efficiency and long-term stability of perovskite solar cells. J Mater Chem A. 2018;6(17):7903.

[33] Laban WA, Etgar L. Depleted hole conductor-free lead halide iodide heterojunction solar cells. Energy Environ Sci. 2013;6(11):3249.

[34] Fan J, Liu C, Li H, Zhang C, Li W, Mai Y. Molecular self-assembly fabrication and carrier dynamics of stable and efficient $CH_3NH_3Pb_{(1-x)}Sn_xI_3$ perovskite solar cells. Chemsuschem. 2017;10(19):3839.

[35] Shi D, Adinolfi V, Comin R, Yuan M, Alarousu E, Buin A, Chen Y, Hoogland S, Rothenberger A, Katsiev K, Losovyj Y, Zhang X, Dowben PA, Mohammed OF, Sargent EH, Bakr OM. Low trap-state density and long carrier diffusion in organolead trihalide perovskite single crystals. Science. 2015;347(6221):519.

[36] Yang Z, Surrente A, Galkowski K, Miyata A, Portugall O, Sutton RJ, Haghighirad AA, Snaith HJ, Maude DK, Plochocka P, Nicholas RJ. Impact of the halide cage on the electronic properties of fully inorganic cesium lead halide perovskites. ACS Energy Lett. 2017;2(7):1621.